ISSN 0018-1439, High Energy Chemistry, 2024, Vol. 58, Suppl. 3, pp. S380–S392. © Pleiades Publishing, Ltd., 2024.

Comparative Analysis of Kinetic Schemes for Simulating DC Micro-Discharges in Helium: from Glow to ARC

A. I. Saifutdinov[a, b, *] and E. V. Kustova[a]

[a] *St. Petersburg State University, St. Petersburg, 199034 Russia*

[b] *Kazan National Research Technical University named after. A.N. Tupolev—KAI, Kazan, 420111 Russia*

**e-mail: as.uav@bk.ru*

Received September 11, 2024; revised September 11, 2024; accepted September 11, 2024

Abstract—This work provides a comparative analysis of the sensitivity of the two most widely used kinetic schemes in helium when simulating various modes of direct current discharges in helium: glow and arc. In particular, a kinetic scheme with the formation of three excited atomic states and one molecular state, as well as a scheme with five excited atomic states and two molecular states, are considered. It is shown that the two models yield different results in the glow discharge mode and similar results in the transition from glow to arc and in the arc mode. A study was carried out of the influence of recombination constants from various databases on the discharge characteristics.

Keywords: glow discharge, arc discharge, microdischarges, atmospheric pressure, helium

DOI: 10.1134/S0018143924701212

INTRODUCTION

Discharges at high pressure, including atmospheric pressure, have attracted increasing attention in the last 10–15 years. This is due to the possibility of their use in new applications related to plasma biomedicine and surface treatment [1–3], analytical chemistry and the development of innovative gas analyzers [4–10], plasma chemistry and the synthesis of nanostructures [11–16]. Based on gas-discharge plasma, various plasmadynamic devices are being developed for aerodynamic and space applications. Here it is worth noting plasma actuators [17–19], the interest in which is associated with their low weight, the possibility of installing electrodes practically without introducing additional disturbances into the flow, the absence of complex mechanical or pneumatic systems, and most importantly, the possibility of installing them directly at the point of origin of undesirable effects: at points of development of disturbances, flow separation, etc. Discharges at high pressure are used in low-thrust plasma engines for modern miniature satellites – cubesats [20, 21].

When developing and optimizing plasma instruments and devices, it is necessary to know the spatial distributions of plasma parameters, as well as the limitations on the input power for generating various discharge modes. Experimental diagnostics of discharges at atmospheric pressure is a difficult task; the set of obtained parameters is limited [5, 6], and their distributions, as a rule, are averaged. In this regard, mathematical modeling and simulation methods are currently used to obtain a comprehensive set of all plasma parameters.

There are various types of discharges to generate plasma at atmospheric pressure. At the same time, direct current discharges remain a convenient testing ground for establishing fundamental mechanisms in gas-discharge plasma, as well as testing methods for its control, and often extrapolating the results obtained to predict plasma parameters in non-stationary discharges.

It should be noted that in recent years a series of works have been published [23–29] devoted to models of direct current discharges, based on a consistent approach to describing the discharge gap and electrodes. Within the framework of this approach, both glow and arc modes were described. Currently, these models are being developed taking into account additional phenomena at the electrode-gas-discharge plasma interface, and the applicability of various sets of plasma-chemical processes is being studied.

Since helium is one of the most commonly used plasma-forming gases in modern gas-discharge devices at atmospheric pressure [5–10, 13, 20–22], the presented work is aimed at conducting a comparative analysis of two kinetic schemes in helium when simulating various modes of direct current discharges. Note that for high-pressure helium in barrier discharges, the strong sensitivity of the modeling results to changes in the constants of certain elementary processes was, in particular, noted in [30].

Table 1. Considered states of helium particles in plasma at high pressure for a first (reduced) set of reactions

No.	Symbol	Energy, eV	Stat. weight	Effective level components
1	He	0	1	1^1S_0
2	He(T)	19.8196	3	$2\,^3S_1$
3	He(S)	20.6157	1	$2\,^1S_0$
4	He*	23.02	36	$3\,^3S_0$, $3\,^1S_1$, $3\,^3P_2^0$, $3\,^3P_1^0$, $3\,^3P_0^0$, $3\,^3D_3$, $3\,^3D_2$, $3\,^3D_1$, $3\,^1D_2$, $3\,^1P_1^0$
5	He^+	24.5874	1	He^+
6	He_2^+	22.24	1	He_2^+
7	He_2^*	17.97	3	He_2^*

MODEL DESCRIPTION

To study plasma parameters in direct current discharges in helium, we used a previously formulated self-consistent model that describes in the frame of the common approach the discharge gap and electrodes [20, 24, 25]. It is based on the continuity equations for charged and excited particles, the electron energy density balance equation, the Poisson equation for determining the electric field and potential, the energy balance equation for the heavy component of the plasma, and the heat equations for the cathode and anode. The complete system of equations can be found in previous works [20, 24, 25].

To analyze the effect of plasma-chemical processes on discharge characteristics, we took as a basis the two most commonly used sets of elementary processes [31–39]. The first took into account the formation of one atomic and molecular helium ion, three excited atomic states and one excited molecular state [28, 31, 32].

The states taken into account are presented in Table 1. The complete set of elementary processes is presented in Table 2.

The second set was based on the plasma-chemical model developed in [33, 34] and taking into account the formation of 5 excited atomic and two molecular states of helium, as well as two types of ions. In addition to those presented in Table 1, additional states considered are presented in Table 3.

It should be noted that the works [31, 33–39] consider various channels of recombination processes, as well as the reaction constants of these processes. In this regard, we analyzed the influence of these processes on the characteristics of DC discharges in various modes. The full set of plasmachemical processes is presented in Tables 4 and 5.

RESULTS

Numerical simulations were carried out for a discharge gap of length $L_g = 1$ mm with tungsten electrodes of length $L_c = L_a = 2$ cm at atmospheric pressure. By varying the ballast resistance in the equation for the circuit, various DC discharge modes were calculated at different current densities.

Numerical calculations were carried out for a reduced set of plasma-chemical reactions presented in Table 2, as well as an expanded one presented in Table 4. Moreover, numerical calculations for an expanded set of plasma-chemical reactions taking into account the recombination processes from [35] and [36] and taking into account the dissociative reaction recombination from [30] gave a quantitatively similar character. Next, we will consider the results of these simulations.

Figure 1 shows the voltage dependences (current-voltage characteristics) for two sets of plasmochemical reactions—reduced (model 1) and extended (model 2) taking into account the recombination reactions from [35], as well as the dependence of the cathode and anode surface temperatures on the current density in the case of a reduced set of elementary processes for a discharge in helium at atmospheric pressure. Note that in the case of an extended set, the dependences of the surface temperature of the cathode and anode on the current density have a similar form, and therefore are not shown in the figure.

It can be seen from the figure that all the main modes of direct current discharges are observed—normal glow (minimum on the current-voltage characteristic in the case of an expanded set of reactions), subnormal glow mode (left branch to a minimum), anomalous glow (increasing current-voltage characteristic from the minimum point), transition from a glow discharge to the arc discharge (declining current-voltage characteristic until it intersects with the dotted line) and the arc discharge itself. In this case, the arc is characterized by two modes, in one of which more intense heating of the cathode is observed, and in the second—more intense heating of the anode.

From a comparative analysis of the current-voltage characteristics for two plasma-chemical sets it is clear

Table 2. The first set of elementary processes in helium plasma

R	Reaction	Reaction constant k_j, m^3/s, or m^6/s, or $1/s$	Description
1	$e^- + He \rightarrow e^- + He$	$f_0(\sigma, w)$	Elastic collision [32, 40]
2	$e^- + He \leftrightarrow e^- + He(T)$		Excitation [32, 40]
3	$e^- + He \leftrightarrow e^- + He(S)$		
4	$e^- + He \leftrightarrow e^- + He^*$		
5	$e^- + He \rightarrow 2e^- + He^+$		Ionization [32, 40]
6	$e^- + He(T) \rightarrow 2e^- + He^+$		Stepwise ionization [32, 40]
7	$e^- + He(S) \rightarrow 2e^- + He^+$		
8	$e^- + He(S) \rightarrow He(T) + e$		Mixing level [32, 40]
9	$e^- + He_2^* \rightarrow He_2^+ + 2e^-$		Stepwise ionization [32, 40]
10	$He(S) + He \rightarrow 2He$	8×10^{-21}	De-excitation [32]
11	$He^* + He \rightarrow He_2^+ + 2e^-$	8×10^{-17}	Associative ionization [32]
12	$He(T) + 2He \rightarrow He_2^* + He$	$8.1 \times 10^{-48} T \exp(-650/T)$	Excimers conversion [31, 35]
13	$He(S) + 2He \rightarrow He_2^* + He$	1.3×10^{-45}	Excimers conversion [31]
14	$He_i^{ex} + He_j^{ex} \xrightarrow{\xi} e^- + He + He^+$ $\xrightarrow{1-\xi} e^- + He_2^+$	$2.9 \times 10^{-15} \left(\frac{T}{293.15}\right)^{0.5}$	Penning ionization* [31]
15	$He^+ + 2He \rightarrow He_2^+ + 2e^-$	$1.4 \times 10^{-43} \left(\frac{T}{293.15}\right)^{-0.6}$	Ion conversion [31]
16	$He^+ + 2e^- \rightarrow He(T) + e^-$	$6.0 \times 10^{-32} \left(\frac{T_e}{T_g}\right)^{-4.4}$	Three-body recombination [35]
17	$He_2^+ + 2e^- \rightarrow He(T) + e^-$	$4.0 \times 10^{-32} \left(\frac{T_e}{T_g}\right)^{-1}$	Three-body recombination [35]
18	$He^+ + e^- + He \rightarrow He(T) + He + e^-$	$1.0 \times 10^{-38} \left(\frac{T_e}{T_g}\right)^{-2}$	Three-body recombination [36]
19	$He_2^+ + e \rightarrow He(T) + He$	$8.9 \times 10^{-9} \left(\frac{T_g}{T_e[K]}\right)^{1.5}$	Dissociative recombination [30]
20	$He_2^+ + e \rightarrow He_2^*$	$5.0 \times 10^{-15} \left(\frac{T_g}{T_e[K]}\right)$	Dissociative recombination [37]
21	$He_2^+ + e^- + He \rightarrow He(T) + 2He$	$5.0 \times 10^{-39} \left(\frac{T_e}{T_g}\right)^{-2}$	Three-body recombination [35]
22	$e^- + He_2^* \rightarrow 2He + e^-$	3.8×10^{-15}	Excimer quenching [31]

* $\xi = 0.3$.

Table 3. Additional states taken into account for the second set of reactions

No.	Symbol	Energy (eV)	Stat. weight	Effective level components
1	He(pT)	20.96	9	$2\,^3P_0^0, 2\,^3P_1^0, 2\,^3P_2^0$
2	He(pS)	21.22	3	$2\,^1P_1^0$
3	He_2^*	17.97	3	$He_2\left(^3\Sigma_u^+\right)$
4	He_2^{**}	18.36	1	$He_2\left(^1\Sigma_g^+\right)$

that both of them describe all discharge modes quite well. At the same time, quantitative differences are observed in the normal glow discharge mode.

For a reduced set of reactions, the voltage across the discharge gap turns out to be lower and amounts to a value slightly greater than 200 V. For an expanded set of reactions, the minimum on the current-voltage characteristic corresponding to the normal mode is more pronounced. In this case, the voltage across the discharge gap in the case of an expanded set of elementary processes turns out to be equal to ~310 V.

The minimum voltage corresponds to a normal discharge with a current density $j \approx 6000$ A/m^2, and for a reduced set of elementary processes this value is less pronounced, but corresponds to the current density $j \approx 634$ A/m^2. Note that both values differ from the reference value of the current density for helium [41], which at room temperature is $j_n \approx 3$ μA/(cm^2 Torr^2). However, if we take into account the heating of the gas, which at the specified value of the current density for an expanded set of elementary processes is 530 K, then from the equation of state of an ideal gas it follows that the gas density changes by ~2 times, and consequently, the normal current density changes from the reference one by almost 4 times. Obviously, in this case, the expanded set gives a closer value to the normal current density. The reduced set gives a very different value, despite the weak heating of the gas. Apparently, this difference is due to the strong influence of nonlinear processes, such as stepwise ionization, Penning ionization, and recombination, which cannot be scaled. Note also that the cathode potential drop in the case of an expanded set of elementary processes is 220 V, while the reference value is ~ 125–150 V. This difference is associated with gas heating and restructuring of the cathode layer due to changes in gas density in this region. On the other hand, a reduced set of reactions with a corresponding normal current density gives a cathode drop of 130 V, which corresponds well to the reference value. Thus, we can draw an intermediate conclusion that when describing the normal regime of a glow discharge, further development of the model is necessary, including taking into account the nonlocality of ionization processes.

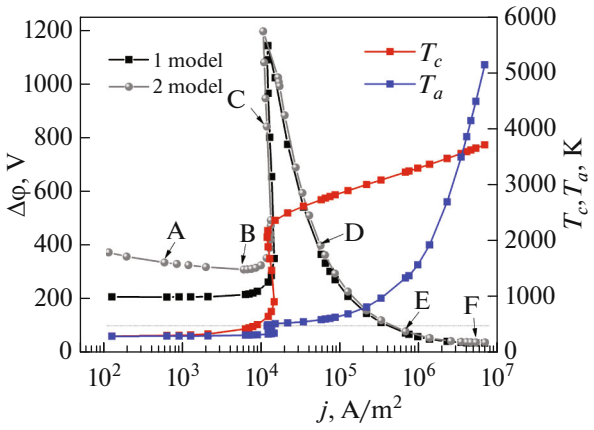

Fig. 1. Dependence of voltage (current-voltage characteristic), cathode and anode surface temperatures on current density in the case of a reduced and expanded set of elementary processes for a discharge in helium at atmospheric pressure.

In an anomalous glow discharge, transition from a glow discharge to an arc discharge, and in an arc discharge mode, the quantitative values of the current-voltage characteristics for both sets of plasma-chemical reactions are practically the same. It should also be noted that in the anomalous mode there is a transition to obstructed discharge—a sharp increase in the discharge voltage with a slight change in the current density. This fact is more clearly expressed in the dependence of the temperature of the electrode surfaces on the current density (S-shaped form). The transition to obstructed discharge is apparently associated with strong heating of the gas in the near-cathode region of the discharge and a decrease in the density of neutral particles.

Figures 2–4 show the distributions of densities of charged and excited particles, electric field and potential, as well as electron temperature and gas temperature at different values of discharge currents corresponding to different modes of a direct current discharge, which are marked in Fig. 1 by points A, B, C, D, E and F.

It can be seen that for point A (Fig. 2 on the left), corresponding to the subnormal glow mode, cathode

Table 4. Second set of elementary processes in helium plasma

R	Reaction	Reaction constant k_j, m^3/s, or m^6/s, or $1/s$	Description
1	$e^- + He \rightarrow e^- + He$	$f_0(\sigma, w)$	Elastic collision [33, 34, 40]
2	$e^- + He \leftrightarrow e^- + He(T)$		Excitation [33, 34, 40]
3	$e^- + He \leftrightarrow e^- + He(S)$		
4	$e^- + He \leftrightarrow e^- + He(pT)$		
5	$e^- + He \leftrightarrow e^- + He(pS)$		
6	$e^- + He \leftrightarrow e^- + He^*$		
7	$e^- + He \rightarrow 2e^- + He^+$		Ionization [33, 34, 40]
8	$e^- + He(T) \rightarrow 2e^- + He^+$		Stepwise ionization [33, 34, 40]
9	$e^- + He(S) \rightarrow 2e^- + He^+$		
10	$e^- + He(pT) \rightarrow 2e^- + He^+$		
11	$e^- + He(pS) \rightarrow 2e^- + He^+$		
12	$e^- + He^* \rightarrow 2e^- + He^+$		
13	$e^- + He_2^* \rightarrow 2e^- + He_2^+$		
14	$e^- + He_2^{**} \rightarrow 2e^- + He_2^+$		
15	$e^- + He(T) \rightarrow He(S) + e^-$		Stepwise excitation [33, 34, 40]
16	$e^- + He(T) \rightarrow He(pT) + e^-$		
17	$e^- + He(T) \rightarrow He(pS) + e^-$		
18	$e^- + He(T) \rightarrow He^* + e^-$		
19	$e^- + He(S) \rightarrow He(Ps) + e^-$		
20	$e^- + He(S) \rightarrow He(Pt) + e^-$		
21	$e^- + He(S) \rightarrow He^* + e^-$		
22	$e^- + He(Ps) \rightarrow He(Pt) + e^-$		
23	$e^- + He(Ps) \rightarrow He^* + e^-$		
24	$e^- + He(Pt) \rightarrow He(Pt) + e^-$		
25	$e^- + He_2^* \rightarrow He_2^{**} + e^-$		
26	$e^- + He_2^* \rightarrow He_2^+ + e^-$		Stepwise ionization [33, 34, 40]
27	$e^- + He_2^{**} \rightarrow He_2^+ + e^-$		
28	$e^- + He_2^* \rightarrow e^- + 2He$	3.8×10^{-15}	Dissociation [33, 34]

Table 4. (Contd.)

R	Reaction	Reaction constant k_j, m^3/s, or m^6/s, or $1/s$	Description
29	$He(T) + 2He \rightarrow He_2^* + He$	$3.23\times10^{-45}\exp(-778/T)$	Excimers conversion [33, 34]
30	$He(S) + 2He \rightarrow He_2^{**} + He$	$3.23\times10^{-45}\exp(-778/T)$	Excimers conversion [33, 34]
31	$He(pT) + 2He \rightarrow He_2^* + He$	$3.23\times10^{-45}\exp(-778/T)$	
32	$He(pS) + 2He \rightarrow He_2^{**} + He$	$3.23\times10^{-45}\exp(-778/T)$	
33	$He^* + 2He \rightarrow He_2^* + He$	$2.42\times10^{-45}\exp(-778/T)$	
34	$He^* + 2He \rightarrow He_2^{**} + He$	$8.0\times10^{-46}\exp(-778/T)$	
35	$He(S) + He \rightarrow He(T) + He$	3.6×10^{-21}	Mixing level [34]
36	$He^* + He \rightarrow He(pT) + He$	$3.204\times10^{-18}T^{0.5}$	
37	$He^* + He \rightarrow He(pS) + He$	$3.204\times10^{-18}T^{0.5}$	
38	$He_i^{ex} + He_j^{ex} \rightarrow e^- + He + He^+ \rightarrow e^- + He_2^+$	$2.9\times10^{-15}\left(\frac{T}{293.15}\right)^{0.5}$	Penning ionization* [31]
39	$He^+ + 2He \rightarrow He_2^+ + He$	$3.017\times10^{-41}T^{-1}$	Ion conversion [31, 37]
40	$He^* + He \rightarrow e^- + He_2^+$	8×10^{-17}	Associative ionization [32]
41	$He(pT) \rightarrow He$	1.0×10^{7}	Radiation [33, 34]
42	$He(pS) \rightarrow He$	1.8×10^{9}	
43	$He^* \rightarrow He$	9.1×10^{7}	
44	$He(pT) \rightarrow He(T)$	1.022×10^{7}	
45	$He(pS) \rightarrow He(S)$	1.97×10^{6}	
46	$He^* \rightarrow He(pT)$	2.94×10^{7}	
47	$He^* \rightarrow He(pS)$	9.79×10^{6}	
	$He_2^{**} \rightarrow 2He$	6.0×10^{8}	

and anode layers, as well as a positive column, are observed.

It should be noted that the cathode layer is quite wide and amounts to slightly more than 0.2 mm. Gas heating in this mode is insignificant; the maximum gas temperature is 323 K.

Upon transition to the normal glow mode, the cathode layer is compressed to 0.046 mm, which, taking into account gas heating to 525 K, practically corresponds to the reference values of the normal thickness of the cathode layer of 1.5 Torr cm [35].

A maximum is formed in the density of electrons and molecular helium ions at a minimum electric field strength. The gas temperature reaches 525 K.

With a further increase in the current density (point C), the density of charged particles increases and a more pronounced maximum is formed in the near-cathode region of the discharge. The dominant type of ions becomes the atomic helium ion. The gas temperature reaches 2000 K, which leads to a significant decrease in the concentration of neutral particles and an increase in sustain voltage to 800 V and higher. A further increase in current density (point D) also leads to an increase in gas temperature and an increase

Table 5. Recombination reactions considered in set 2 of plasma-chemical reactions

R	Reaction	Reaction constant k_j, m^3/s, or m^6/s, or $1/s$	Reference
Three-body recombination			
48	$He_2^+ + 2e \rightarrow \begin{cases} He_2^* + e \\ He(T) + e \\ He(S) + e \\ He_2^{**} + e \end{cases}$	$\begin{cases} - \\ 100\% \quad 4.0\times10^{-20}\left(\frac{T_g}{T_e}\right)^4 \\ - \\ - \end{cases}$	[35]
		$\begin{cases} 75\% \\ 25\% \quad 4.0\times10^{-20}\left(\frac{T_g}{T_e}\right)^4 \\ - \\ - \end{cases}$	[36]
		$\begin{cases} 5.4\times10^{-27}T_e^{-4.5} \\ - \\ - \\ 3.59\times10^{-27}T_e^{-4.5} \end{cases}$	[33, 34]
		$\begin{cases} - \\ 100\% \quad 1.1\times10^{-14}\left(\frac{T_g^{2.3}}{T_e^{4.5}}\right) \\ - \\ - \end{cases}$	[38]
50	$He_2^+ + e + He \rightarrow \begin{cases} He(2\,^1P) + 2He \\ He(2\,^3P) + 2He \\ He(2\,^1S) + 2He \\ He(2\,^3S) + 2He \\ He_2^{**} + He \end{cases}$	$\begin{cases} - \\ - \\ - \quad 5.0\times10^{-27}\left(\frac{T_g}{T_e}\right)^{1\pm1} \\ 70\% \\ - \end{cases}$	[35]
		$\begin{cases} 25\% \\ 75\% \quad 1.0\times10^{-26}\left(\frac{T_g}{T_e}\right)^2 \\ - \\ - \\ - \end{cases}$	[36]
		$\begin{cases} - \\ - \\ - \\ 1.0\times10^{-31}T_e^{-3.5} \\ 4.156\times10^{-29}T_e^{-1.5} \end{cases}$	[33, 34]

Table 5. (Contd.)

R	Reaction	Reaction constant k_j, m^3/s, or m^6/s, or $1/s$	Reference
51	$He^+ + 2e \rightarrow$ $He(2\,^1P) + e$ $He(2\,^3P) + e$ $He(2\,^1S) + e$ $He(2\,^3S) + e$ $He^* + e$	– – – 100% – $\quad 6.0\times10^{-20}\left(\frac{T_g}{T_e}\right)^4$	[35]
		19% 56% 6% 19% – $\quad 6.0\times10^{-20}\left(\frac{T_g}{T_e}\right)^4$	[36]
		– – $1.4\times10^{-27}T_e^{-4.5}$ $4.1\times10^{-27}T_e^{-4.5}$ $3.59\times10^{-27}T_e^{-4.5}$	[33, 34]
		– – – 100% – $\quad 1.1\times10^{-14}\left(\frac{T_g^{2.3}}{T_e^{4.5}}\right)$	[38]
52	$He^+ + e + He \rightarrow$ $He^* + He$	$4.156\times10^{-29}T_e^{-1.5}$	[33, 34]
Dissociative recombination			
49	$He_2^+ + e \rightarrow$ $He^* + He$ $He(2\,^1P) + He$ $He(2\,^3P) + He$ $He(2\,^1S) + He$ $He(2\,^3S) + He$	– – – 50% 50% $\quad 8.9\times10^{-9}\left(\frac{T_g}{T_e[K]}\right)^{1.5}$	[30]
		$5.0\times10^{-10}\,T/T_e$ – – $3.0\times10^{-11}T_e^{-1.5}$ –	[33, 34]

in cathode temperature. The thermionic emission mechanism is turned on and the discharge begins to burn in the transition mode from a glow discharge to an arc.

At a current density corresponding to point E, the discharge begins to burn in arc mode, while the voltage across the discharge drops to 70–80 V, and the cathode layer is compressed to 6–10 microns. The density of charged particles reaches the following values: $n_e \approx n_i \approx 10^{21}$ m^{-3}. With a further increase in the current density, the cathode potential drop decreases, gas heating increases and intense heating of the anode is observed. It can be seen that at a current density cor-

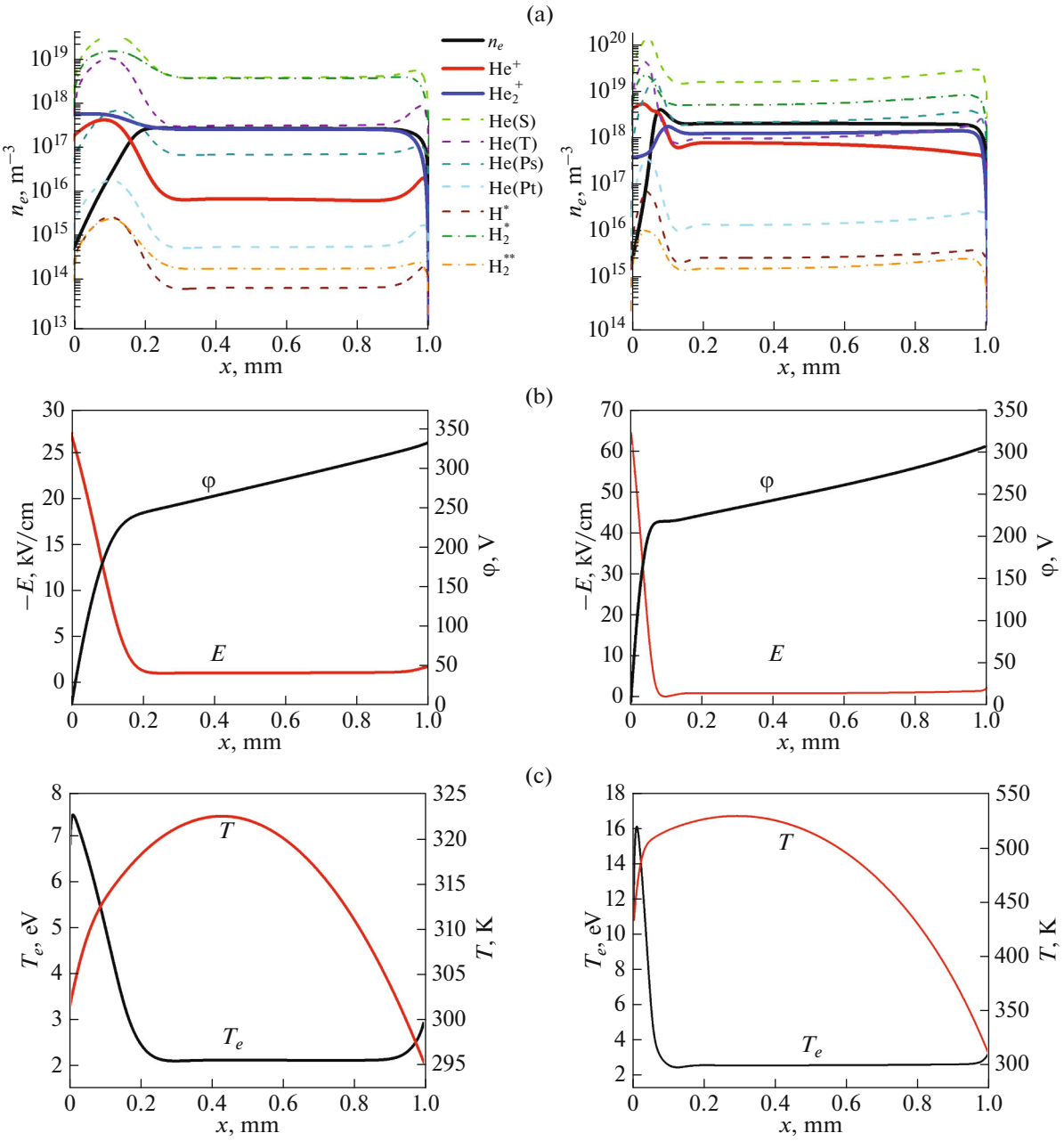

Fig. 2. Distribution of (a) density of charged and excited particles, (b) electric field and potential, (c) electron temperature and temperature of heavy gas particles for current densities corresponding to point A (on the left) and point B on the right in Fig. 1.

responding to point F in an arc discharge, the anode temperature is higher than the cathode temperature.

Further we the influence of various three-body and dissociative recombination constants on the discharge characteristics. As shown by numerical simulations, the main differences were in the region of a normal glow discharge. Figure 5 shows the distributions of densities of charged particles, electric field and potential in the case when the recombination constants were taken from work I [30, 36], II [30, 38] and III [33, 34].

Note that the recombination constants from [30, 36] give almost similar values as [30, 35] (see Figs. 2a and 2b). The dominant ion species is molecular helium, which is typical for high-pressure discharges. When using the recombination constants from [30, 38], the dominant type of ions becomes atomic helium, which is more typical for discharges at low pressures or at high temperatures (as in the case of arc discharges). In the case of recombination constants from [33, 34], the dominant ion is also the molecular

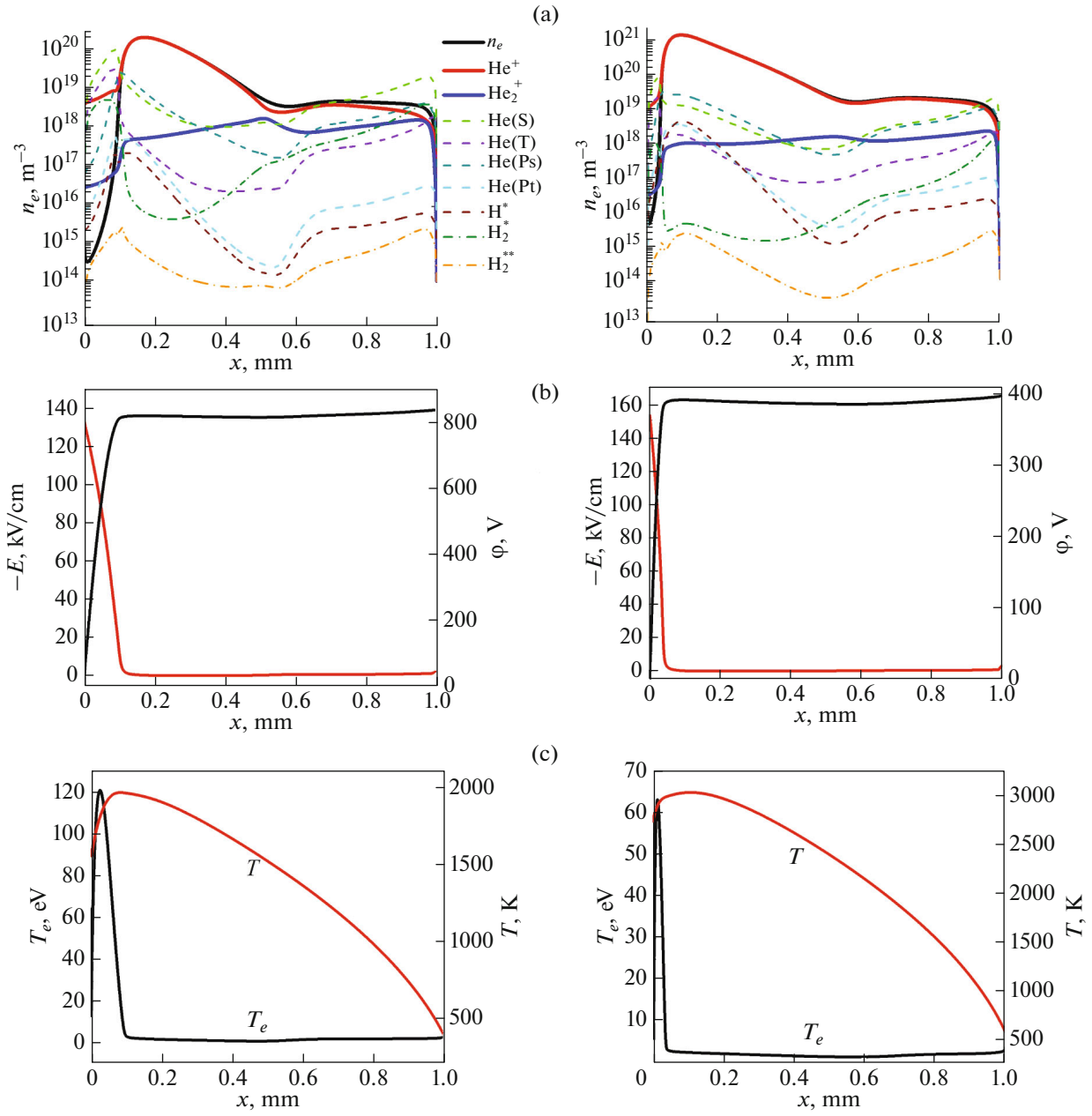

Fig. 3. Distribution of (a) density of charged and excited particles, (b) electric field and potential, (c) electron temperature and temperature of heavy gas particles for current densities corresponding to point C (on the left) and point D on the right in Fig. 1.

helium ion, but the density of the atomic helium ion turns out to be extremely underestimated. A comparative analysis of potential distributions shows that in the case of using recombination constants from various works, it shows that in all cases the cathode potential drop is the same. However, the potential drop in the discharge gap turns out to be ~260 V when using the constants from [33, 34]. In addition, we note that a more pronounced minimum of the electric field in the negative glow region appears when using the constants from [30, 36] and [30, 38].

Thus, the question of using different recombination constants remains open and requires a more detailed analysis and comparison with experimental data obtained through probe and optical measurements.

CONCLUSIONS

Numerical simulations are carried out to study the influence of various sets of plasma-chemical reactions on the characteristics of direct current discharges in

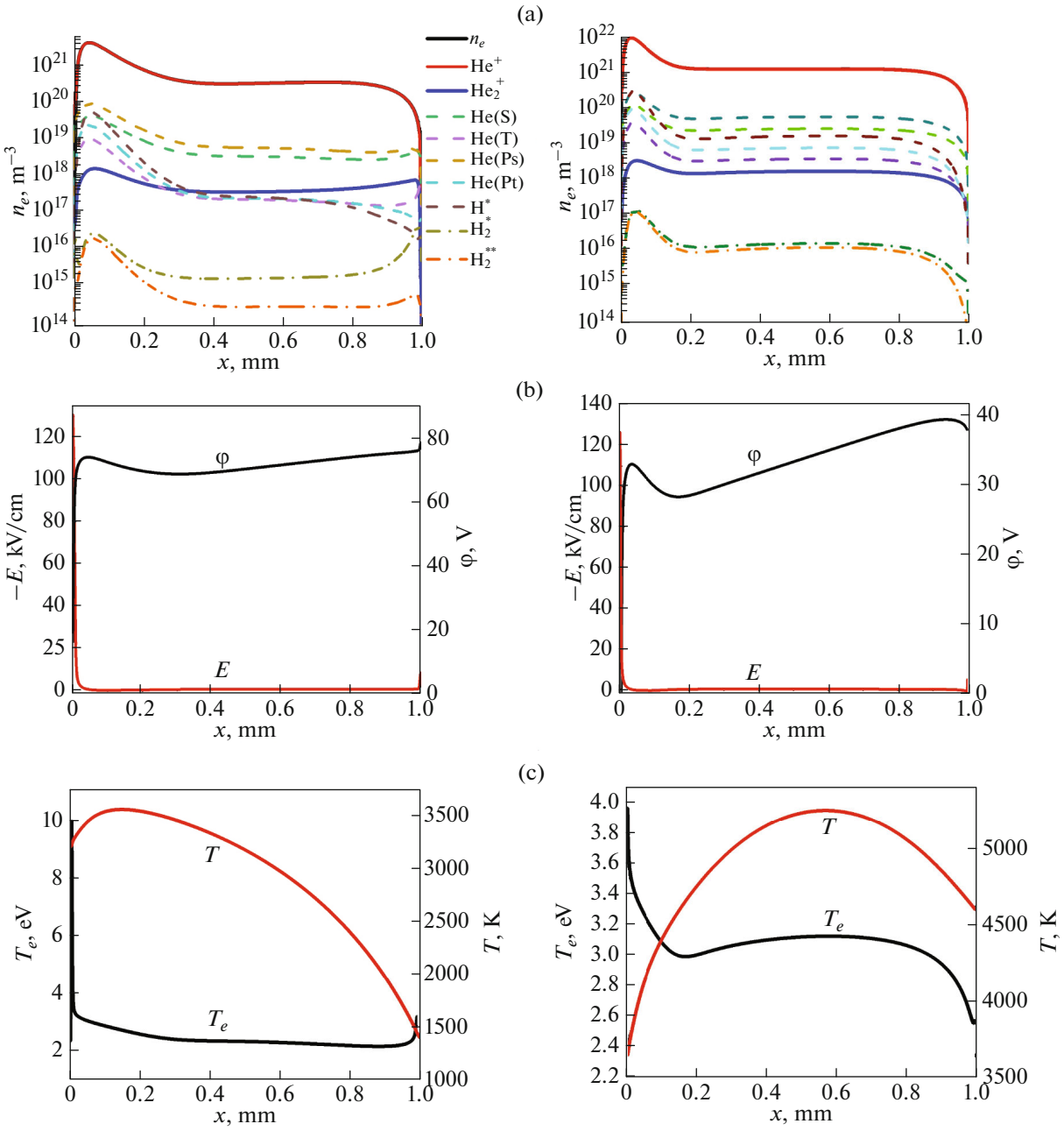

Fig. 4. Distribution of (a) density of charged and excited particles, (b) electric field and potential,(c) electron temperature and temperature of heavy gas particles for current densities corresponding to point E (on the left) and point F on the right in Fig. 1.

various modes: from glow to arc. It is shown that taking into account additional atomic excited levels leads to a more correct reproduction of the normal glow mode. Moreover, in the anomalous, transitional from the anomalous glow (and obstructed) to the arc mode, and in the arc mode, the reduced and expanded sets give quantitatively similar discharge characteristics. The sensitivity of the choice of three-body and dissociative recombination constants for the characteristics of a normal glow discharge has been studied.

FUNDING

The research was supported by a grant from the Russian Science Foundation, project no. 23-19-00241, https://rscf.ru/project/23-19-00241/.

CONFLICT OF INTEREST

The authors of this work declare that they have no conflicts of interest.

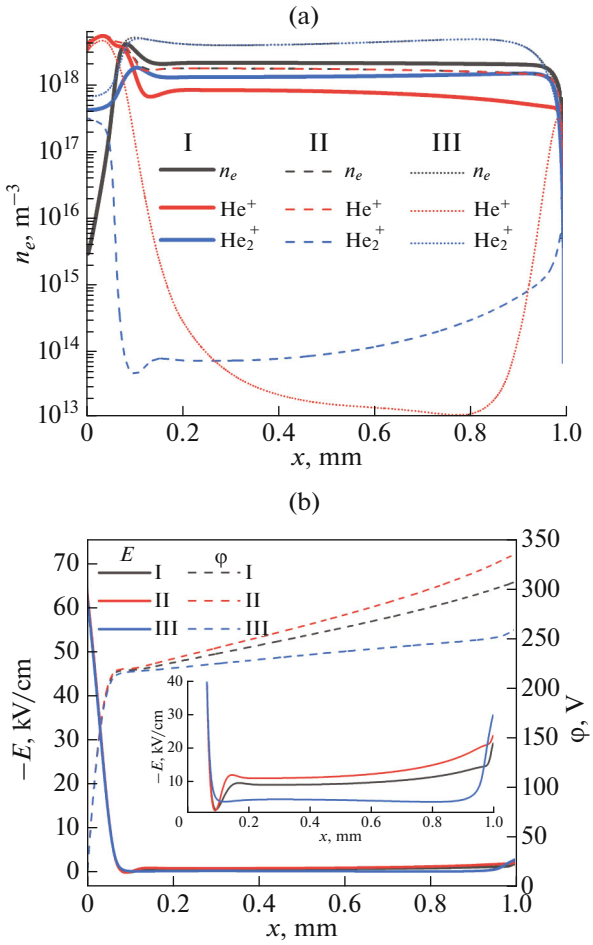

Fig. 5. Comparative analysis in the distributions of the density of charged particles, as well as the electric field strength and potential for an expanded set of elementary processes, taking into account the recombination constants from work I [30, 36], II [30, 38] and III [30, 34], respectively.

REFERENCES

1. Zhang, B., Sun, Y., Han, W., et al., *Plasma Sources Sci. Technol.*, 2023, vol. 32, no. 7, p. 075020.
2. Zhao, L.-X., Zhao, H.-X., Chen, H., Hu, C., Zhang, Y., and Li, H.-P., *Plasma Chem. Plasma Process.*, 2023, vol. 43, no. 6, p. 1567.
3. Xia, G. et al., *IEEE Trans. Plasma Sci.*, 2014, vol. 42, no. 10, p. 2768.
4. Kudryavtsev, A.A., Stefanova, M.S., and Pramatarov, P.M., *J. Appl. Phys.*, 2015, vol. 117, p. 133303.
5. Yuan, C., Kudryavtsev, A.A., Saifutdinov, A.I., et al., *Phys. Plasmas*, 2018, vol. 25, p. 104501.
6. Saifutdinov, A.I. and Sysoev, S.S., *Plasma Sources Sci. Technol.,* 2021, vol. 30, p. 017001.
7. Zhou, C., Yao, J., Saifutdinov, A.I., et al., *Plasma Sources Sci. Technol.*, 2022, vol. 31, p. 107001.
8. Zhou C. et al., *Physics of Plasmas*, 2024, vol. 31, no. 5.053510.
9. Zhou, C., Yao, J., Saifutdinov, A.I., et al., *Plasma Sources Sci. Technol.*, 2021, vol. 30, no. 11, p. 117001.
10. Saifutdinov, A.I. and Sysoev, S.S., *Plasma Sources Sci. Technol.*, 2023, vol. 32, no. 11, p. 114001.
11. Lin, L. and Wang, Q., *Plasma Chem. Plasma Process.*, 2015, vol. 35, p. 925.
12. Mariotti, D. and Sankaran R.M., *J. Phys. D: Appl. Phys.*, 2010, vol. 43, no. 32, p. 323001.
13. Ng, J. and Raitses, Y., *J. Appl. Phys.*, 2015, vol. 117, no. 6, p. 063303.
14. Timerkaev, B.A., Kaleeva, A.A., Timerkaeva, D.V., and Saifutdinov, A.I., *Russ. J. Phys. Chem. A*, 2020, vol. 94, no. 3, p. 613.
15. Lebedev, Yu.A., Averin, K.A., Borisov, R.S., et al., *High Energy Chem.*, 2018, vol. 52, no. 4, p. 324. https://doi.org/10.1134/S0018143918040100
16. Lebedev, Y.A., Tatarinov, A.V., and Epstein, I.L., *Plasma Chem. Plasma Process.*, 2019, vol. 39, p. 787. https://doi.org/10.1007/s11090-019-09975-8
17. Kuryachii, A.P., Rus'yanov, D.A., and Skvortsov, V.V., *Uch. Zap. TsAGI*, 2011, vol. 42, no. 2, p. 68.
18. Gamirullin, M.D., Kuryachii, A.P., Litvinov, V.M., and Chernyshev, S.L., *Uch. Zap. TsAGI*, 2014, vol. 45, no. 6, p. 28.
19. Lapushkina, T.A., Erofeev, A.V., Azarova, O.A., and Kravchenko, O.V., *Tech. Phys.*, 2019, vol. 89, no. 1, p. 34.
20. Lee, J. and Raja, L.L., *J. Appl. Phys.*, 2024, vol. 135, no. 17, p. 0190223.
21. Abaimov, M.D., Micci, M.M., and Bilén, S.G., A 17.8-GHz microwave electrothermal thruster for CubeSats and small satellites, *Proceedings of the IEPC 2016, Cambridge, MA, USA, 17 August 2016.*
22. Kurbanismailov, V.S., Maiorov, S.A., Omarov, O.A., and Ragimkhanov, G.B., *Tech. Phys.*, 2019, vol. 64, no. 3, p. 348.
23. Saifutdinov, A.I., Fairushin, I.I., and Kashapov, N.F., *JETP Lett.*, 2016, vol. 104, no. 3, p. 180.
24. Baeva, M., Loffhagen, D., and Uhrlandt, D., *Plasma Chem. Plasma Process.*, 2019, vol. 39, p. 1359.
25. Baeva, M., Loffhagen, D., Becker, M.M., and Uhrlandt, D., *Plasma Chem. Plasma Process.*, 2019, vol. 39, no. 4, p. 949.
26. Saifutdinov, A.I., *J. Appl. Phys.*, 2021, vol. 129, no. 9, p. 093302.
27. Saifutdinov, A.I., *Plasma Sources Sci. Technol.*, 2022, vol. 31, no. 9, p. 094008.
28. Saifutdinov, A.I., Germanov, N.P., Sorokina, A.R., and Saifutdinova, A.A., *Plasma Phys. Rep.*, 2023, vol. 49, no. 10, p. 1187.
29. Saifutdinov, A. and Timerkaev, B., *Nanomaterials*, 2023, vol. 13, no. 13, p. 1966.
30. Golubovskii, Yu.B., Maiorov, V.A., Behnke, J., and Behnke, J.F., *J. Phys. D: Appl. Phys.*, 2003, vol. 36, no. 1, p. 39.
31. Wang, Q., Economou, D.J., and Donnelly, V.M., *J. Appl. Phys.*, 2006, vol. 100, no. 2, p. 023301.
32. Donko, Z., Hartmann, P. and Kutasi, K., *Plasma Sources Sci. Technol.*, 2006, vol. 15, p. 178.

33. Bogdanov, E.A., Kapustin, K.D., Kudryavtsev, A.A., and Chirtsov, A.S., *Tech. Phys.*, 2010, vol. 55, no.10, p. 1430.

34. Rafatov, I., Islamov, G., Eylenceoglu, E., Yesil, C., and Bogdanov, E., *Phys. Plasmas*, 2023, т. 30, no. 9, p. 093504.

35. Deloche, R., Monchicourt, P., Cheret, M., and Lambert, F., *Phys. Rev. A*, 1976, vol. 13, no. 3, p. 1140.

36. Emmert, F., Angermann, H.H., Dux, R., and Langhoff, H., *J. Phys. D: Appl. Phys.*, 1988, vol. 21, no. 5, p. 667.

37. Alves, L.L., Gousset, G., and Ferreira, C.M., *J. Phys. D: Appl. Phys.*, 1992, vol. 25, no. 12, p. 1713.

38. Belmonte, T., Cardoso, R.H., Henrion, G., and Kosior, F., *J. Phys. D: Appl. Phys.*, 2007, vol. 40, no. 23, p. 7343.

39. Santos, M., Noel, C., Belmonte, T., and Alves, L.L., *J. Phys. D: Appl. Phys.*, 2014, vol. 47, no. 26, p. 265201.

40. Alves, L.L., Bartschat, K., Biagi, S.F., et al., *J. Phys. D: Appl. Phys.*, 2013, vol. 46, no. 33, p. 334002.

41. Raizer, Yu.P., *Fizika gazovogo razryada* (Gas Discharge Physics), Dolgoprudnyi: Intellekt, 2009, 3rd ed.